Supplemental Information

Insight into the structural evolution mechanism and potassium storage performance of expanded graphitic onion-like carbon

Chenyang Meng,[a] Man Yuan,[a] Bin Cao,[b] Zipeng Jiang,[a] Jiapeng Zhang,[a] Ang Li,[a] Xiaohong Chen,[a] Mengqiu Jia*[a] and Huaihe Song*[a]

[a.] *State Key Laboratory of Chemical Resource Engineering, Beijing Key Laboratory of Electrochemical Process and Technology for Materials, Beijing University of Chemical Technology, Beijing, 100029, P. R. China.*

[b.] *College of Material Science and Engineering, Xi'an University of Science and Technology, Xi'an, Shanxi Province 710054, China.*

E-mail: jiamq@mail.buct.edu.cn, songhh@mail.buct.edu.cn.

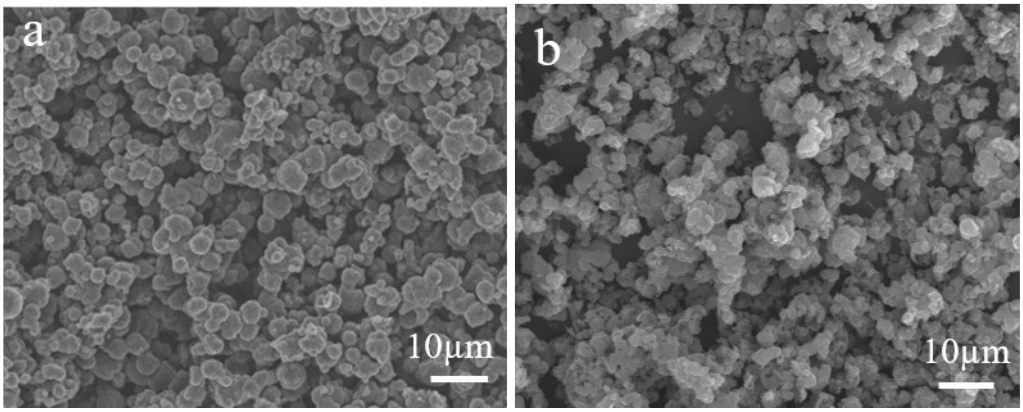

Fig. S1. SEM micrographs of (a) GOC and (b) O-GOC.

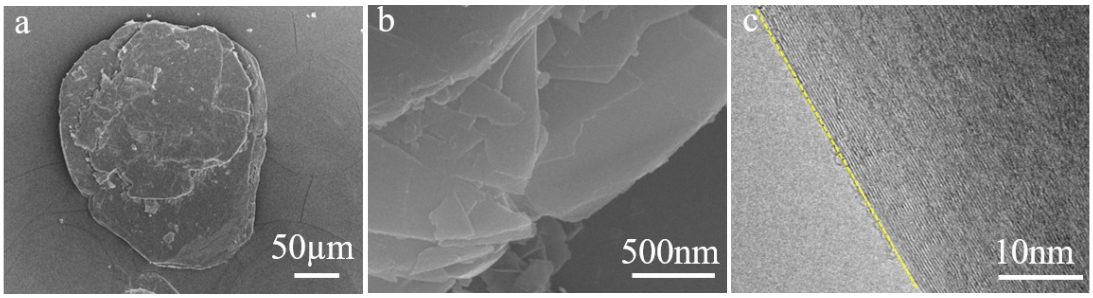

Fig. S2. (a, b) SEM images and (c) TEM image of NFG.

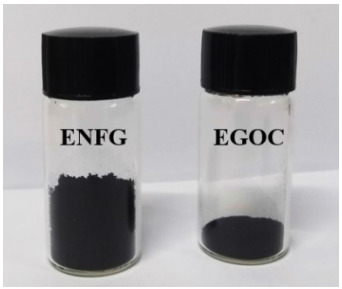

Fig. S3. Photograph of ENFG and EGOC with the same weight of 20 mg.

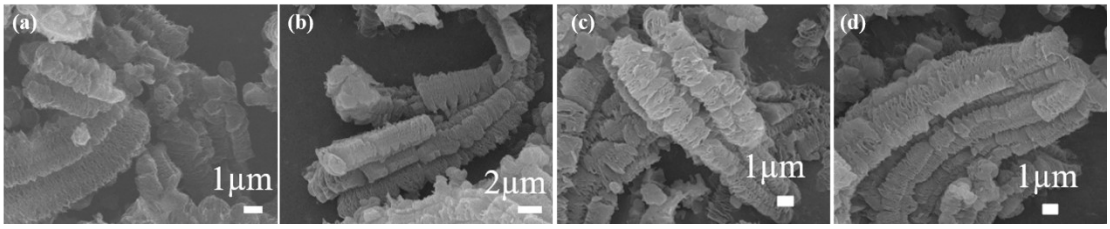

Fig. S4. Morphology and structure characterizations. SEM images of the (a) EGOC200, (b) EGOC300, (c) EGOC400 and (d) EGOC500.

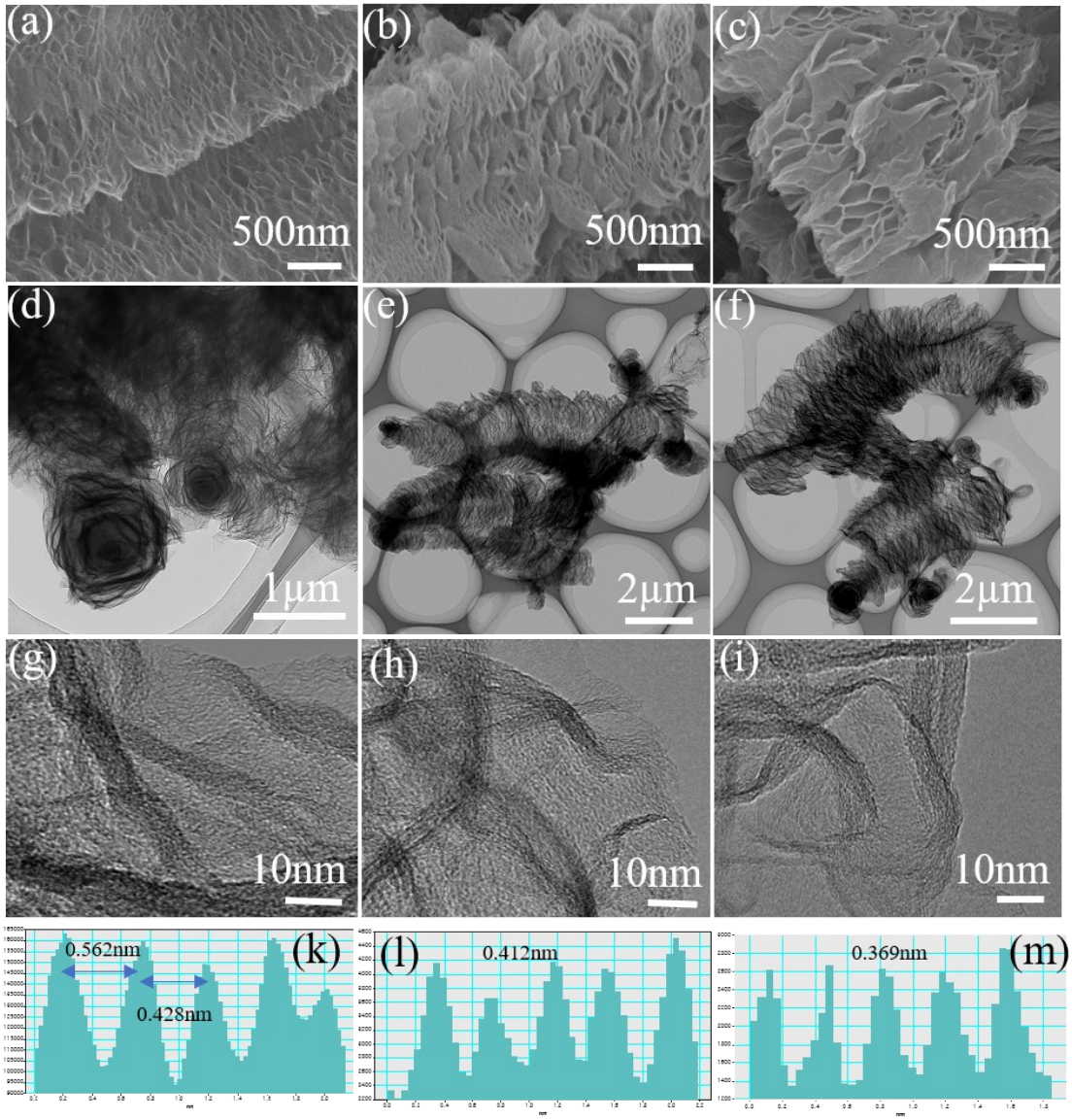

Fig. S5 (a-c) SEM images, (d-f) TEM images, (g-i) HRTEM images and (k-m) the calculated interlayer spacing of EGOC200, EGOC300 and EGOC500.

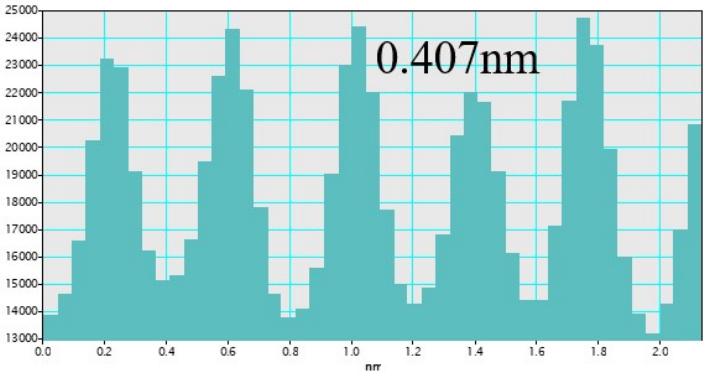

Figure. S6 The calculated interlayer spacing of Figure 2f.

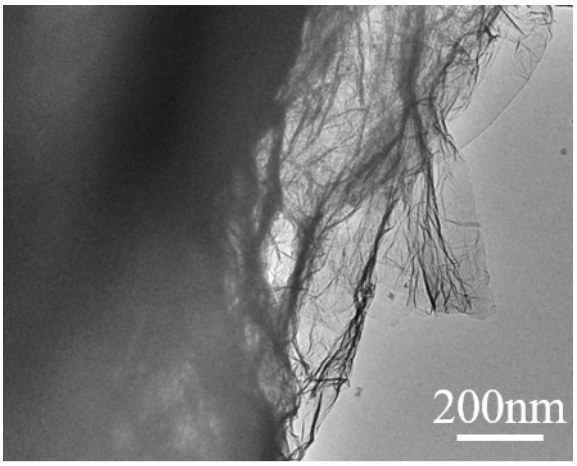

Fig. S7 TEM images of ENFG400 without ultrasound treatment.

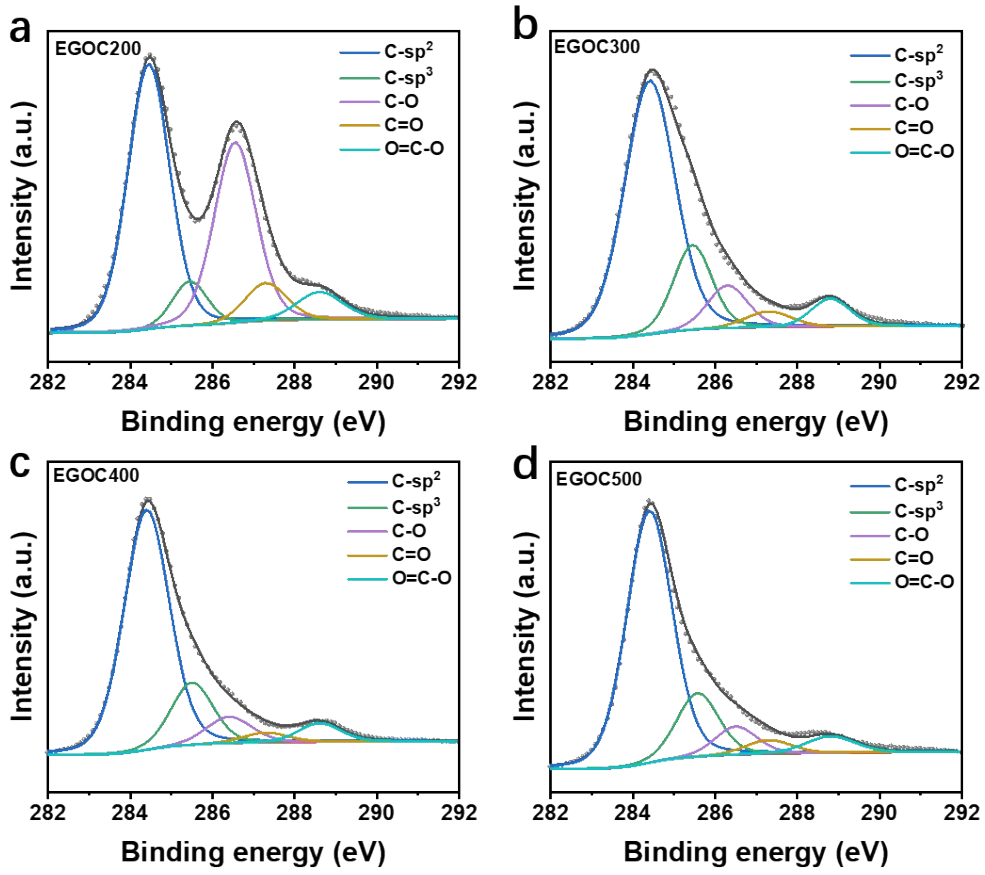

Fig. S8 High-resolution C1s spectra of (a) EGOC200, (b) EGOC300, (c) EGOC400 and (d) EGOC500.

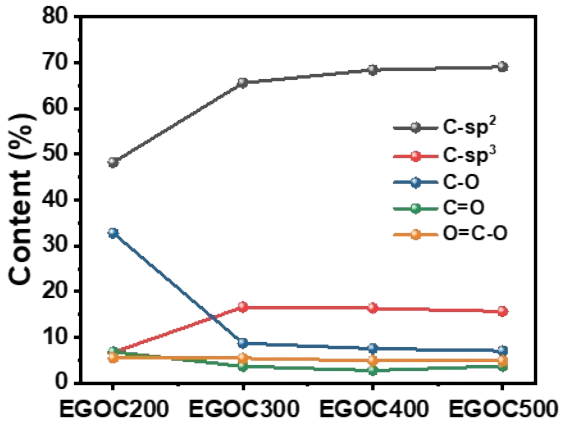

Fig. S9 Variation of the C-sp^2, C-sp^3, C-O, C=O and O=C-O values of EGOC200, EGOC300, EGOC400 and EGOC500.

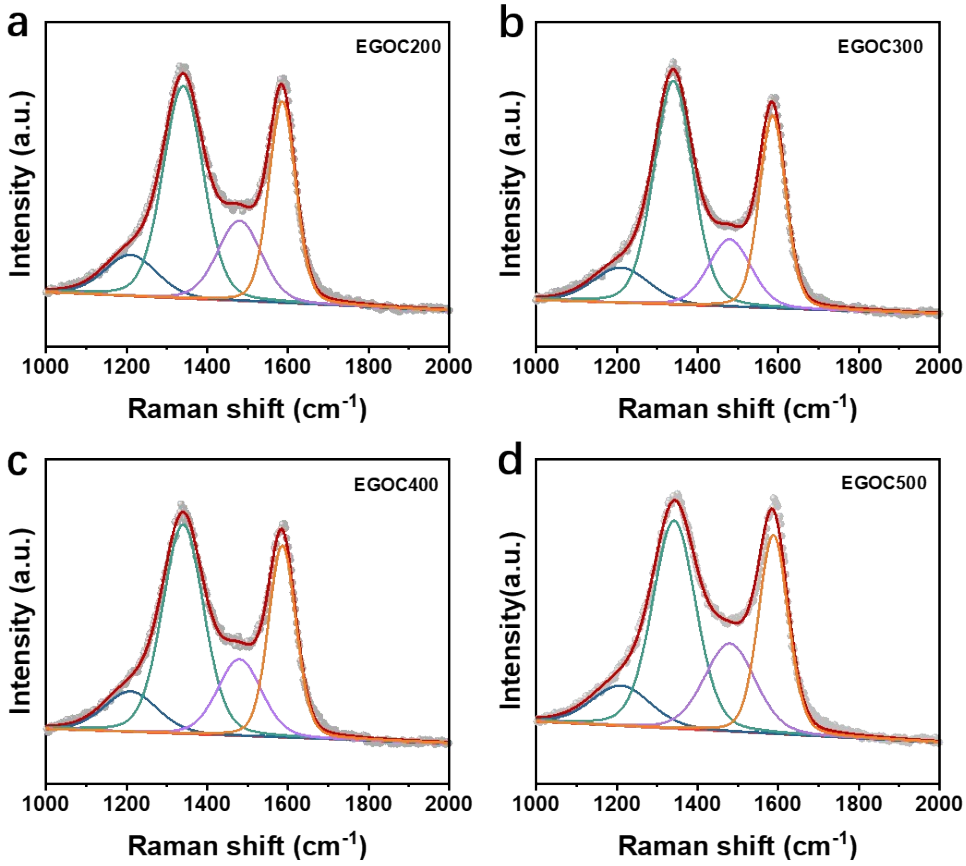

Fig. S10 Raman spectra of (a) EGOC200, (b) EGOC300, (c) EGOC400 and (d) EGOC500.

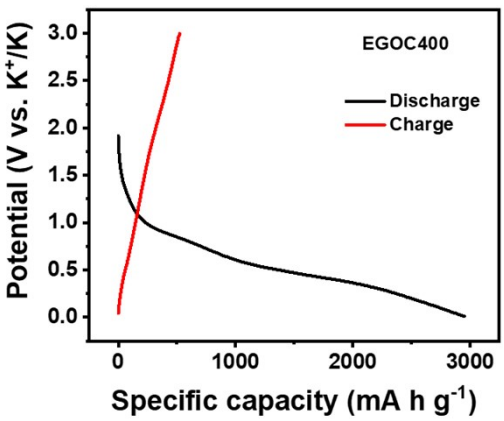

Fig. S11 Galvanostatic charge discharge curves for the first cycle of EGOC400.

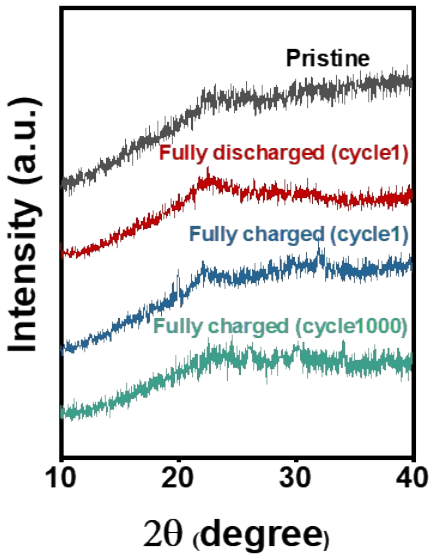

Fig. S12 The XRD of EGOC400 during potassiation/depotassiation process at different states: pristine, potassiated to 0. 01 V in the first cycle, depotassiated to 3.0 V in the first cycle and fully charged after1000cycle.

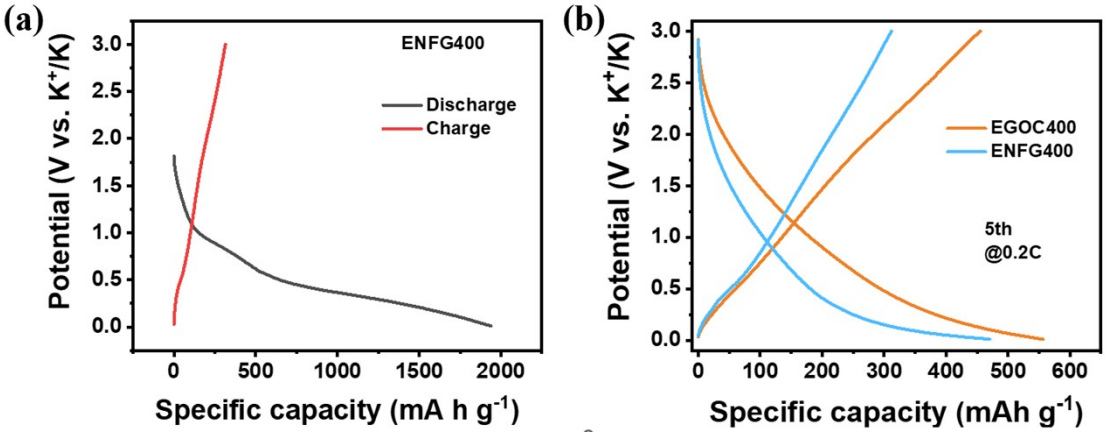

Fig. S13 Galvanostatic charge discharge curves for (a) the first cycle of ENFG400, and (b) the fifth cycle of EGOC400 and ENFG400.

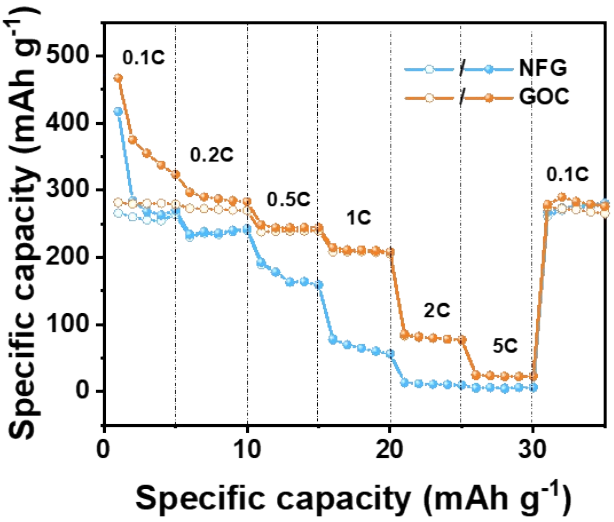

Fig. S14 The rate performance of EGOC400 and ENFG400.

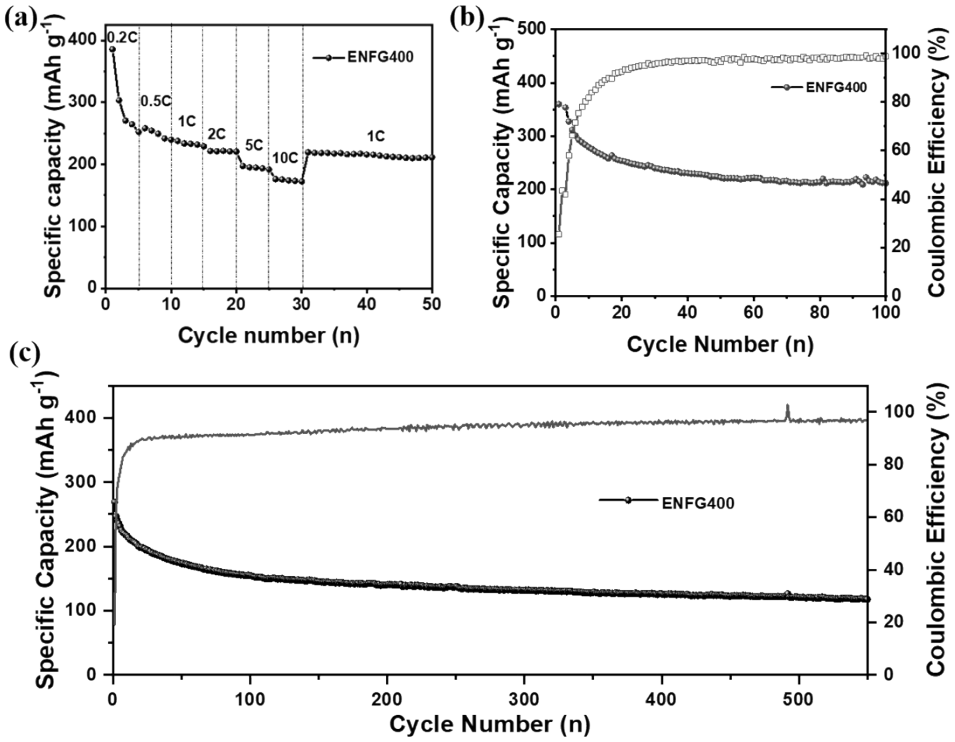

Fig. S15 (a) Rate performance of ENFG400. Cycling performance of ENFG400 at (b) 0.2C and (c) 2C.

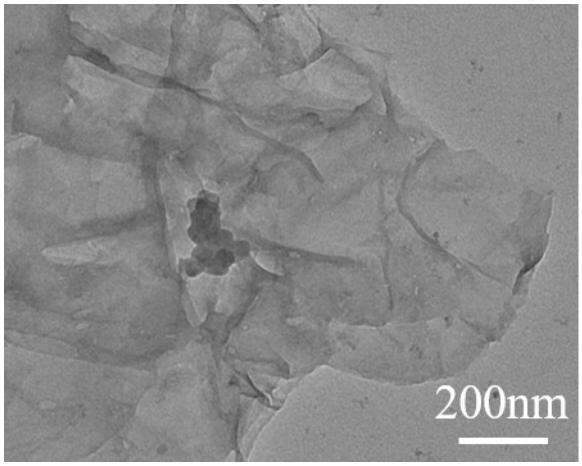

Fig. S16 TEM image of the ENFG400 after 500 cycles.

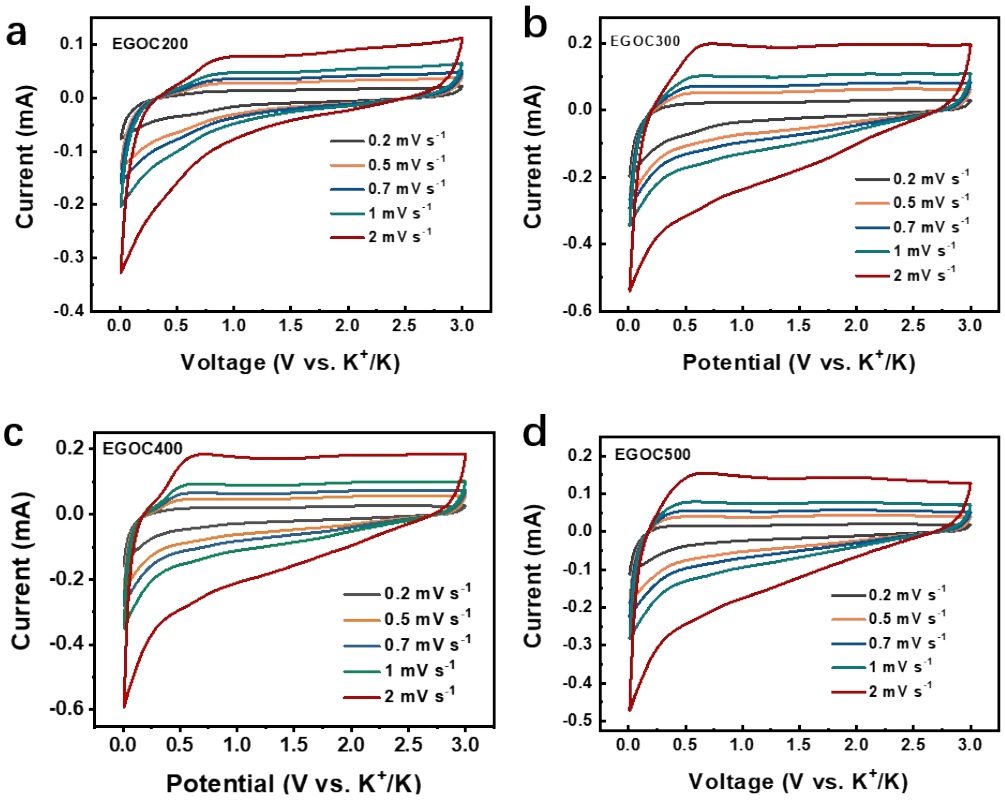

Fig. S17 CV curves at various scan rates of (a) EGOC200, (b) EGOC300, (c) EGOC400 and (d) EGOC500.

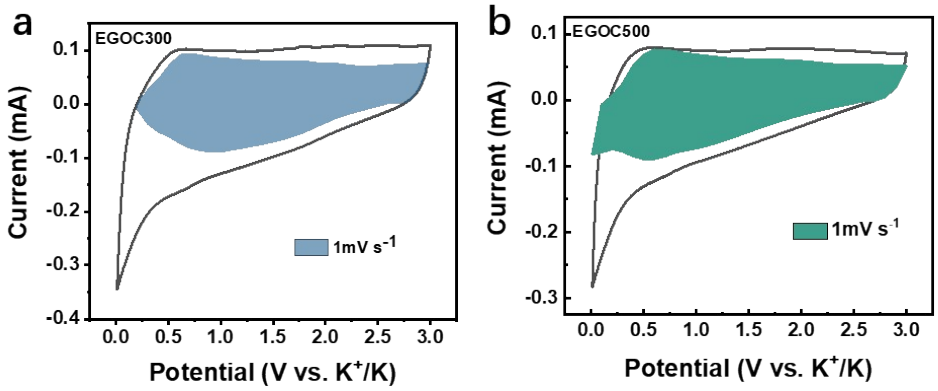

Fig. S18 The capacitive contribution at 1 mV s^{-1} of (a) EGOC300 and (b) EGOC500.

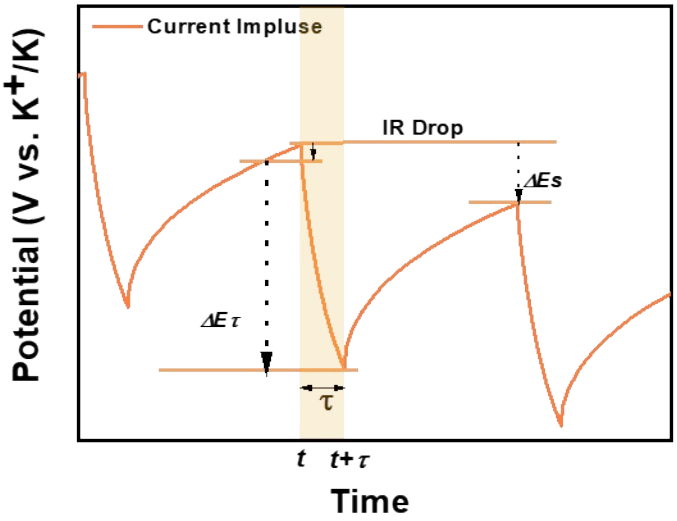

Fig. S19 Determination of ΔEτ and ΔEs from the measured GITT profiles.

The K^+ diffusion coefficient in EGOC electrodes can be calculated by solving Fick's second law using the following equation:

$$D = \frac{4}{\pi\tau}\left(\frac{m_B V_m}{M_B S}\right)^2\left(\frac{\Delta E_s}{\Delta E_\tau}\right)^2$$

where τ is the relaxation time, m_B is electrode active mass, M_B is the molar mass of the electrode material for carbon, V_M is the molar volume of carbon, S is the

geometric area of the electrode, ΔE_s is the steady-state potential charge by the current pulse and ΔE_τ is the potential charge during the constant current pulse.

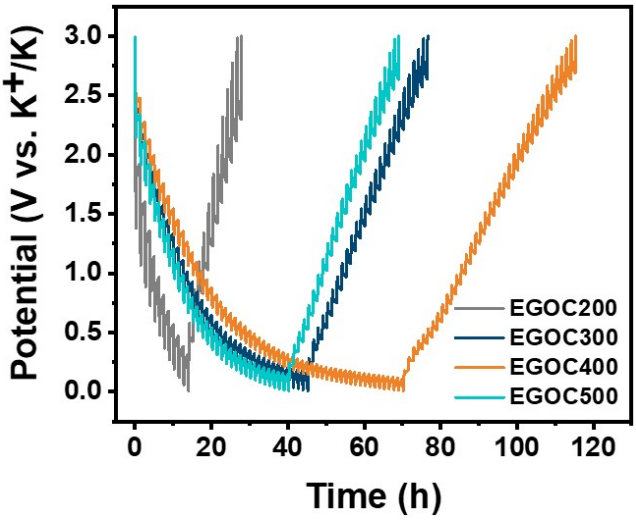

Fig. S20 GITT profiles at various potassiation/depotassiation voltages in first cycle for EGOC200, EGOC300, EGOC400 and EGOC500.

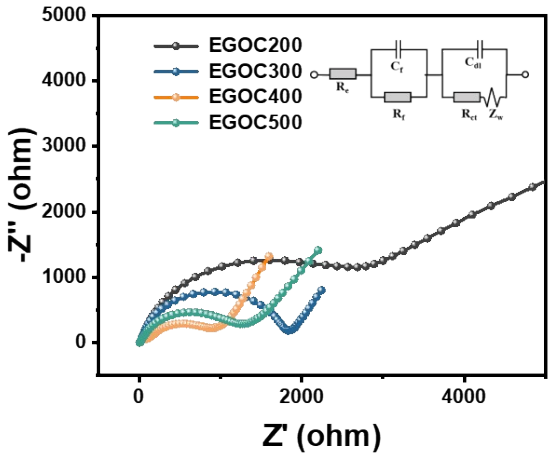

Fig. S21 EIS plots of EGOC200, EGOC300, EGOC400 and EGOC500 at open-circuit voltage.

The energy density and power density of PIC were calculated using the following equations:

$$E = \int_{t1}^{t2} UI/mdt$$

$$P = \frac{E}{t} \times 3600$$

where I, U, m, t_1, and t_2 are assigned to the discharge current (A), operating voltage (V), total mass of active materials (g), start and end times of the discharge (s), respectively, and t is t_1- t_2.

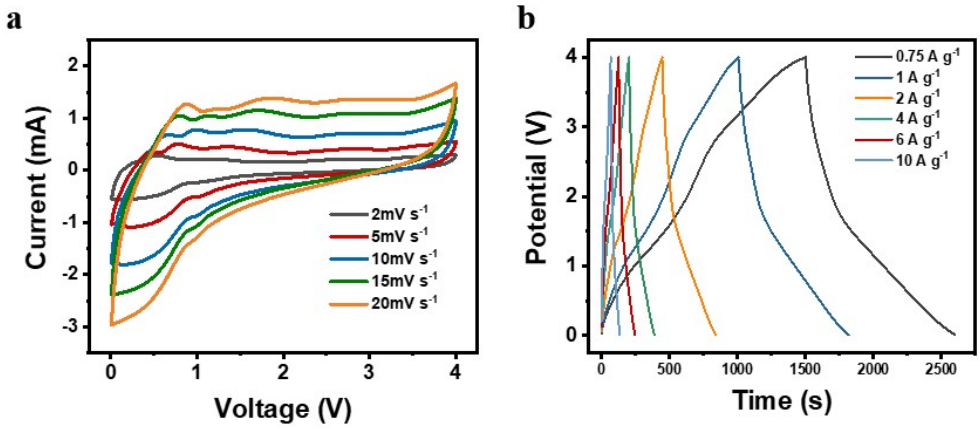

Fig. S22 (a) The CV curves at different scan rates and (b) galvanostatic charge–discharge profiles at various current densities of the (-) REGOC//AC (+) PIC.

Table S1. The structural parameters of GOC and NFG.

Samples	d_{002} (nm)	L_a (nm)	L_c (nm)	G (%)
GOC	0.3384	52.34	24.02	65.60
NFG	0.3361	91.27	31.06	91.83

Table S2. The C and O contents of the as-prepared EGOC at different temperature by XPS analysis.

Samples	C (at%)	O at%	C-SP^2 (%)
EGOC200	71.07	28.93	48.18
EGOC300	83.74	16.26	65.55
EGOC400	85.19	14.81	68.38
EGOC500	86.09	13.91	69.03

Table S3. Textual parameters of EGOC.

sample	[a] S_{BET}	[b] V<2nm	[c] V<50nm	[d] V>50nm	[e] V_{DFT}
	$m^3\ g^{-1}$	$m^3\ g^{-1}$	$m^3\ g^{-1}$	$m^3\ g^{-1}$	$m^3\ g^{-1}$
EGOC200	103.34	0.165	0.148	0.259	0.572
EGOC300	369.17	0.44	0.894	0.413	1.351
EGOC400	573.40	0.067	1.37	1.509	2.496
EGOC500	449.09	0.054	1.128	0.466	1.648

a: The BET specific surface area; b: Pore volume of micropores calculated by DFT; c: Pore volume of 2 nm<d<10 nm calculated by DFT; d: Pore volume of 10 nm<d<50 nm calculated by DFT; e: Pore volume of macropores calculated by DFT; f: The total DFT pore volume.

Table S4 Kinetics parameters of PCNSs

sample	R_e	R_f	R_{ct}
EGOC200	6.12	18.8	298.3
EGOC300	5.74	13.47	164.1
EGOC400	5.15	11.65	147.54
EGOC500	5.66	12.89	157.7